Allosteric Control and Glycan Shielding Adaptations in the SARS-CoV-2 Spike from Early to Peak Virulence

Authors

Srirupa Chakraborty,[1],* , Kien N. Nguyen,[2] Mingfei Zhao[3], S. Gnanakaran[4]*

Affiliations

[1] Department of Chemical Engineering, Northeastern University, Boston, MA 02115

[2] Cresset, Cambridgeshire, SG80SS, UK

[3] Department of Chemical and Biological Engineering, The University of Alabama, Tuscaloosa, AL 35487

[4] Theoretical Biology and Biophysics, Los Alamos National Laboratory, Los Alamos, NM 87545

* co-corresponding author: s.chakraborty@northeastern.edu

* co-corresponding author: gnana@lanl.gov

27   **ABSTRACT**

28

29   The SARS-CoV-2 Spike glycoprotein is central to viral infectivity and immune evasion, making

30   it a key target for vaccine and therapeutic design. This trimeric peplomer undergoes dynamic

31   conformational changes, particularly in its Receptor Binding Domain (RBD), which transitions

32   between closed (down) and ACE2-accessible (up) states relative to the rest of the protein, to

33   facilitate host cell entry. Structural understanding of such critical inter-domain motions, as well as

34   epitope exposure quantification, is essential for obtaining an effective molecular handle over this

35   protein and, in turn, exploiting it towards improved immunogen development. Focusing on the

36   early circulating D614G form and the later emerging Delta (B.1.617.2) variant with higher

37   virulence, we performed large-scale molecular dynamics simulations of the soluble form of the

38   Spike in both 'down' and 'up' conformations of the RBD. Guided by differences in overall

39   fluctuations, we described reaction coordinates based on domain rotations and tilting to extract

40   features that distinguish D614G versus Delta structural behavior of the N-terminal Domain (NTD)

41   and RBD. Using reaction coordinate analysis and Principal Component Analysis (PCA), we

42   identify allosteric coupling between the N-terminal Domain (NTD) and RBD, where NTD tilting

43   influences RBD gating. While some of these motions are conserved across variants, Delta exhibits

44   an optimized RBD-gating mechanism that enhances ACE2 accessibility. Additionally, glycan

45   remodeling in Delta enhances shielding at the NTD supersite, contributing to reduced sensitivity

46   to neutralizing antibodies. Finally, we uncover the impact of the D950N mutation in the HR1

47   region, which modulates downstream Spike dynamics and immune evasion. Together, our findings

48   reveal variant-specific and conserved structural determinants of SARS-CoV-2 Spike function,

49   providing a mechanistic basis for allosteric modulation, glycan-mediated immune evasion, and

50   viral adaptation. These insights offer valuable guidance for rational vaccine and therapeutic design

51   against SARS-CoV-2 and emerging variants.

52

INTRODUCTION

Viruses, more notably RNA viruses, constantly undergo mutations that can evolve into new variants and strains[1, 2]. While most of these variants have minimal impact and disappear quickly, others can affect transmissibility, virulence, and vaccine effectiveness, persisting as variants of concern through natural selection. Since its discovery in December 2019, the Severe Acute Respiratory Syndrome Coronavirus 2 (SARS CoV-2) has accumulated several mutations. Based on the WHO epidemiological updates, SARS CoV-2 went through many Variants of Concern (such as the Alpha, Beta, Gamma, Delta, and Omicron lineages), along with several Variants of Interest for the SARS CoV-2[3, 4]. While Omicron out-competed other previous variants in global dissemination through its high transmissibility[5, 6], the Delta variant exhibited higher virulence, symptom severity, increased hospitalization, and long-COVID associations[7-9].

A large fraction of these mutations occur on the Spike peplomers expressed at the surface of the virus. This glycoprotein, which aids in host cell recognition, fusion, and cellular ingress[10], is the primary exposed viral antigen and is critical for triggering varieties of host immune responses[11]. Inversely, the Spike protein itself participates in immune evasion through glycan shielding and garnering mutations. Understanding the structure and dynamics of this protein and the effects of the emerging mutations is critical to improving immunogen design and treatment strategies that target viral entry.

The SARS CoV-2 Spike protein is a homotrimer, each of which accommodates two bulky and dynamic globular domains at the apical region – the N-terminal Domain (NTD) and the Receptor Binding Domain (RBD) (**Fig 1**). Both these domains have been found to prompt a large panel of antibodies, housing some critical epitopes[12, 13]. This manifestly indicates that obstructing the dynamics and functions of these domains can prevent the overall functioning of the virus. While it is known that the RBD transitions between ACE2-inaccessible "down" and ACE2-binding compatible "up" conformations[14], along with insights into some of the structural determinants of these transitions[15, 16], broader allosteric regulation of RBD dynamics, particularly its coupling with the NTD and other Spike domains, remains incompletely understood. The NTD has remained even more cryptic in terms of its structure-function relations. The relatively narrow base of the Spike has the furin cleavage site (FCS) with the RRAR motif on each protomer

3

83 that separates the S1-S2 subunits[17]. The base also includes the heptad repeat helices HR1 and

84 HR2, typical of class I fusion proteins.

85   A lot of experimental efforts have been expended to obtain details of the Spike protein

86 structure through numerous studies[14, 18-22]. These, however, only manage to capture the static

87 conformations of the protein in a small number of stable states. These proteins are dynamic entities,

88 where not only the large-scale transitional motions but even the equilibrium fluctuations are critical

89 elements that drive function. Exemplifying this are the effects of some emergent mutations over

90 the last few years. While many of these sequence modifications can be easily interpreted by local

91 structural changes[20, 22-25] and attributed to direct interaction outcomes (antibody escape or

92 enhanced receptor affinity)[26-28], some important mutations are located away from known

93 epitopes and ACE2 binding site. These mutations do not cause sizeable structural modifications,

94 yet affect the Spike behavior through substantial alterations to essential dynamics and allosteric

95 effects. A notable example is the single amino acid substitution D614G[29] located on an

96 unstructured loop, away from key structural domains such as NTD, RBD, FCS and the HRs. Yet,

97 by a cascade of structural dynamics, the D614G causes a higher probability of RBD opening[30,

98 31] and enhanced infection capability[29, 32], resulting in this substitution being the dominant

99 variant.

100   The collective motions of NTD and RBD in SARS-CoV-2 variants have drawn interest due

101 to their regulatory role in the functional change of Spike and potential drug-binding ability.[24,

102 33-36] Melero et al. have characterized NTD-RBD movements to a large degree as a rotation using

103 a consensus-based image-processing approach with principal component analysis, but they also

104 identified an important structural rearrangement from a complex pattern of flexibility presented by

105 different RBDs.[35] Using molecular dynamics simulations, Li et al. found the neighboring NTD

106 prohibits the RBD's movements as a wedge detaches and swings away, leading to the potential

107 binding target of NTD-RBD interface.[34] Choi et al. also used long all-atom simulations to study

108 motions of the RBD and the NTD in fully glycosylated systems and non-glycosylated systems

109 with full-length Spike in a viral membrane.[25] Wang et al. investigated conformational change

110 of Delta Spike protein using molecular simulations to capture a "breath" motion initiated by an

111 RBD swing movement, in which the three inter-protomer NTD-RBD pairs tilt outward and

112 downward simultaneously.[24]

113   While numerous SARS-CoV-2 variants emerged over the course of the pandemic, the Delta

114   variant is a crucial model for understanding viral evolution, structural adaptability, and immune

115   evasion strategies. Unlike later variants, such as Omicron, which prioritized increased

116   transmissibility at the cost of virulence, Delta exhibited a uniquely severe disease phenotype,

117   contributing to higher hospitalization rates and mortality compared to both its predecessors and

118   successors[8]. Notably, Delta's defining mutations, including L452R, T478K, and P681R,

119   enhanced its infectivity, RBD dynamics, and immune escape mechanisms, some of which persist

120   in later Omicron sublineages[37]. Through its impact, Delta can serve as a benchmark for studying

121   allosteric regulation, glycan-mediated shielding, and structural plasticity in SARS-CoV-2,

122   providing insights that extend beyond a single variant and inform future vaccine and therapeutic

123   design. The Delta (B.1.617.2) variant has 10 mutations on the Spike, over and above the D614G

124   variant as depicted in **Fig. 1** — T19R,T95I,G142D,E156del,F157del and R158G in the NTD,

125   L452R,T478K in the RBD, P681R near the FCS, and D950N at the base of the HR1 helix. Another

126   salient feature of the Spike is that there are ~22 N-glycans (as well as a few putative O-glycans)[38,

127   39] present on the surface of the protein that provide immune shielding and operational controls

128   by virtue of their dynamics[40-42], which cannot be fully resolved by current experimental

129   techniques. To better understand the functional nuances of these mutations and glycans,

130   computational modeling of the detailed dynamics of this glycoprotein is the way forward. Findings

131   from such simulations can provide a thorough understanding of the effects of emerging mutations

132   as well as the innate dynamic properties that should remain invariant.

133   In this article, we investigate how the inter-domain dynamics between RBD and NTD vary

134   between two different variants, Delta and the D614G (called G614 from here on). The latter variant

135   is one of the major early substitutions on the original Wuhan strain, which was widely probed in

136   terms of structure-dynamics relationships[20, 30, 40, 43]. To dissect how mutations can affect

137   Spike function as well as extract the innate structural invariants that drive the peplomer behavior,

138   we performed extensive all-atom explicit-solvent molecular dynamics (MD) simulations of the

139   G614 and Delta Spike. For each of these variants, the '1-up' and 'all-down' conformations

140   (indicating the up/down orientation of RBD relative to the Spike) were modeled with native

141   glycosylation patterns[39]. We begin by studying the glycan shielding of the Spike protein surface

142   and how the virus evolved to optimize the shielding effect over critical regions. Guided by

143   differences in overall fluctuations, we further define cardinal reaction coordinates based on

144 NTD/RBD rotations and tilting to extract features that distinguish variant-dependent structural
145 behavior and consequently establish the dynamic links that drive concerted motions between these
146 two important domains. We go on to utilize Principal Component Analyses to extract the most
147 significant dynamical cross-correlations between these domains and explain them in terms of the
148 glycan modifications. Finally, we end with a detailed analysis of epitope exposure and
149 vulnerability at the conserved immuno-critical regions of the fusion peptide[44] and the heptad
150 repeat regions[45, 46]. These results have equipped us with robust engineering capabilities to
151 overcome vaccine and Spike-targeting therapeutic design challenges.

152

153 **RESULTS**

154

155 The extensive MD simulations reported in this study include natively glycosylated Spike
156 soluble ectodomain trimer of the G614 and Delta variants with the same glycoforms[39]. Each of
157 these two variants was simulated in both all-RBD down (ACE2 inaccessible) and 1-RBD up
158 (ACE2 binding compatible) conformations with five independent microsecond-long trajectories
159 (total simulation time of 20μs; see SI Methods for details). In order to distinguish between the
160 three similar protomers in the Spike, we will refer to them as chains A, B, and C (counter-clockwise
161 arrangement), where chain B is open in the 1-RBD up system, chain A is to the left and chain C is
162 to the right of the up chain B (see **Fig.1**).

163

164 **Enhanced Glycan Shielding of the NTD in the Delta Variant Reduces Antibody**
165 **Accessibility**
166
167 Here, we quantify the effective glycan shielding by employing the glycan-encounter-factor
168 (GEF) metric designed by us earlier[30, 47], which essentially measures the relative glycan
169 coverage encountered by an approach probe (an antibody, for example) over each residue on the
170 protein surface, taking the glycan and protein dynamics into account. To provide an overview of
171 how this glycan coverage may alter between variants, we calculated the residue-wise difference in
172 GEF values (Delta minus G614) for the entire Spike (**Fig. S1**). The differences are most
173 noteworthy in the NTD region, where glycan shielding across this domain is notably higher for the
174 Delta variant, relative to G614 over a large area of contiguous protein surface (**Fig. S1**). To further
175 illustrate this, **Fig. 2** shows the average GEF (calculated from all three protomers) as a function of

176   NTD residues for the G614 and Delta simulations. In particular, NTD surfaces spanned by residues

177   ~100 to 190 and ~230 to 280 exhibit significantly higher coverage by glycans in the Delta variant,

178   as compared to G614 (**Fig. 2a/b/c**). We note that these NTD surfaces include residues from the

179   NTD supersite and epitopes of most NTD-specific neutralizing antibodies[48, 49]. Hence, the

180   increased glycan shielding in these NTD areas could help the Delta variant evade NTD-targeting

181   antibodies.

182   To elucidate additional contributors to NTD-antibody binding, we calculated the solvent-

183   accessible surface area (SASA), for the NTD supersite that defines epitopes for most NTD-specific

184   antibodies[49]. Changes in SASA would capture surface exposure variations because of protein

185   structural burial. Interestingly, the SASA values remain similar in the NTD supersite for the G614

186   and Delta variants (**Fig. S2**). This suggests that the numerous modifications in the Delta NTD do

187   not have any significant perturbation to the solvent-accessible surface area (SASA) of the NTD

188   supersite. Rather, those Delta mutations modulate the orientations of the glycans, leading to

189   enhanced glycan shielding of the NTD. Together, the results (cf. **Figs. S1, 2, S2**) corroborate the

190   important role of the glycans that allow the Delta variant to become more evasive to NTD-directed

191   antibodies. This finding is of critical concern since this corroborates and rationalizes previous

192   evidence that NTD-specific monoclonal antibodies have reduced sensitivity for the Delta

193   variant[50, 51].

194

Restricted RBD Flexibility in Delta Facilitates ACE2 Accessibility

196

197   Since the viral RBD is responsible for binding to the host receptor, the dynamics of RBD

198   are critical for how infectious a variant may be. To explore this aspect, we first checked the Root

199   Mean Squared Fluctuations (RMSF) of the RBD residues (**Fig. S3**). Predictably, the overall RMSF

200   of the up-RBD (protomer B) is significantly higher, in G614 (**Fig. S3b**). This is not unexpected

201   since the RBD in the up conformation has a lesser number of interactions with neighboring protein

202   domains to stabilize it. However, an interesting feature that emerges here indicates that the up-

203   RBD is relatively more rigid (i.e. less flexible) in the Delta (**Fig. S3d**). To understand this

204   difference further, we look into the essential dynamics of the RBD. We defined simple reaction

205   coordinates that capture (i) an opening and (ii) a twisting movement of the RBD (see SI Methods

206   and **Figs. S4, S5, 3**). To compare the simulated RBD dynamics, we calculated 2D distributions

207   along RBD opening and twist, for all trajectories of G614 and Delta (**Figs. S4, S5, 3**). We find that

208 the most significant difference between these variants is in the up-RBD conformation of protomer

209 B (**Fig 3**). Specifically, the up-RBD of G614 samples a larger conformational space (leading to

210 higher flexibility, **Figs. 3, S3**) than the up-RBD of Delta. Further, the dominant up-RBD ensembles

211 (i.e. the locations of free-energy minima) differ between G614 and Delta, where the G614 up-RBD

212 on average adopts greater opening and twisting angles than the Delta up-RBD, which is confined

213 to a basin of smaller opening and twisting values (**Fig. 3**).

214   To explore the biological implications of these RBD differences, we discuss how the

215 distinct orientations of the up-RBD (in protomer B) may impact the opening movement of the

216 neighboring RBD (in protomer A). For this, we chose two nearest-to-mean configurations where

217 each represents the dominant up-RBD ensemble of the G614 and Delta simulations, respectively

218 (**Fig. S6**). In these representative 1-up G614 and 1-up Delta structures, we then model an identical

219 up-RBD in the neighboring protomer A, which is otherwise in the down orientation (see SI

220 Methods). This allows us to infer how the up-transition of the protomer-A RBD may be affected

221 by the variant-specific up-RBD orientations in the adjacent protomer B (cf. **Fig. 3**). In the G614

222 Spike, the up-RBD of protomer B, due to its the large opening angle and twist (cf. **Fig. 3b**), is

223 positioned closer to the neighboring RBD of protomer A (**Fig. S6**). This apparently introduces

224 steric hindrance that impedes the up-transition of the adjacent protomer-A RBD (**Fig. S6**). By

225 contrast, in the Delta Spike, a smaller opening angle and twist (cf. **Fig. 3c**) allow the up-RBD of

226 protomer B to remain further away from the neighboring RBD. This reduces potential steric

227 clashes and likely facilitates the up-movement of the adjacent RBD in protomer A (**Fig. S6**).

228 Together, these results expound the structural bases of observed Delta RBD structural diversity

229 and increased population of 2-up or 3-up RBD configurations[52, 53], which would conceivably

230 facilitate virus-host binding, thereby enhancing the infectivity of Delta, as compared to G614.

231

NTD Tilting in Delta Influences RBD Orientation and Gating

233
234   Since each NTD can interact with an RBD of a neighboring protomer, it is instructive to

235 also characterize the motion of NTD, in order to establish any correlated dynamics between

236 adjacent NTD/RDB pairs. To this end, we defined structural coordinates that measure i) a tilting

237 and ii) a torsion movement of the NTD (**Fig. 4a**). To compare the simulated NTD dynamics, 2D

238 distributions along NTD tilting and torsion were computed for all trajectories (Figs. **S7, S8, 4b/c**).

239 We find that the most notable difference between G614 and Delta is in the protomer C for the 1-

240   up Spikes (**Fig. 4b/c**). The calculations demonstrate that the NTD can undergo large-scale

241   rotational motions that are variant-specific. The G614 and Delta variants have distinct dominant

242   NTD orientations in their respective protomer C (**Fig. 4b/c**) – the protomer where the NTD is

243   structurally adjacent to the up-RBD (protomer B). Overall, the Delta NTD appears to sample a

244   larger conformational space and adopts more tilted orientations, compared to G614 (**Fig. 4b/c**).

245   The variant-specific NTD dynamics in protomer C (of 1-up G614/Delta; cf. **Fig. 4b/c**) is

246   related to the variant-specific RBD dynamics in protomer B (cf. **Fig. 3b/c**). To interpret this, note

247   that the NTD of protomer C (or C-NTD) is nearest to the RBD up-protomer (protomer B or B-

248   RBD). The other adjacent pairs are B-NTD/A-RBD and A-NTD/C-RBD (cf. **Fig. 1**), where A-

249   RBD and C-RBD are RBD down-protomers in the 1-up Spike. Interestingly, the B-NTD and A-

250   NTD, which are adjacent to RBD down-protomers, are overall more localized (i.e. less mobile),

251   remaining at smaller NTD tilting and torsion angles (**Fig. S7**). This suggests that there is a

252   stabilizing effect between an RBD down-protomer (**Fig. S4**) and its neighboring NTD (**Fig. S7**).

253   By contrast, the C-NTD, adjacent to the up B-RBD, undergoes a wider range of tilt and torsion

254   motions (**Fig. 4b/c**). Further, the distinct rearrangements of this C-NTD between G614 and Delta

255   (**Fig. 4b/c**) appear to be associated with the variant-specific up B-RBD dynamics (**Fig. 3b/c**). This

256   C-NTD/up B-RBD relationship is plausible because the numerous mutations in the NTD

257   apparently alters the rearrangements of the NTD (cf. **Fig. 4b/c**), which likely impacts the

258   orientation of its direct neighbor, the up-RBD (**Fig. 3b/c**).

259

Glycan-Mediated Coupling of NTD and RBD Modulates Spike Conformations

262   Earlier, we discussed how the numerous modifications in the NTD can alter glycan

263   orientations, leading to distinct glycan shielding of the NTD surface (cf. **Fig. 2**). In addition, the

264   analysis of **Fig. 4** suggests that those NTD mutations also affect large-scale NTD rotations. These

265   changes in NTD rearrangements (cf. **Fig. 4b/c**), together with the shift in glycan orientations (cf.

266   **Fig. 2**), may influence the conformation of the neighboring up-RBD, which is characteristic of

267   each Spike variant (cf. **Fig. 3**). To identify which glycans mediate the C-NTD/up B-RBD

268   correlation (cf. **Figs. 3, 4**), we calculated the glycan conformational space for the dominant up-

269   RBD ensembles (corresponding to the high occupancy basins) of the G614 and Delta trajectories

270   (cf. **Fig. 3b/c**), respectively. We then visually compare the resultant glycan densities between those

271   G614 and Delta ensembles in order to determine which glycans differ in orientation for different

272 variants. Based on how they are positioned on the protein surface, these glycans may contribute to

273 the correlated movement of the C-NTD and up B-RBD.

274 Near the up B-RBD, we find that glycans N165 and N234 in the adjacent C-NTD, and

275 glycan N331 in the up B-RBD sample different orientations in the G614 and Delta simulations

276 (**Fig. 5**). Specifcally, a comparison of these simulations suggests that these three glycans cling to

277 (and move with) the up B-RBD, which appears to accommodate (and influence) the specific up B-

278 RBD orientations observed in the G614 and Delta simulations (**Fig. 5**). Glycans N165 and N234

279 have been previously shown to strongly affect Spike opening[15], with N165 increasing and N234

280 decreasing RBD up conformations[54] in the original Wuhan strain. Even glycan N331, located at

281 the base of the RBD, can affect receptor binding[55] and antibody response[56]. Our simulations

282 indicate that these glycans lodge at the base of the RBD in different orientations, and stabilize

283 disparate RBD conformations.

284 These results demonstrate how mutations in the NTD, and glycans, can have far-reaching

285 implications for the function of the Spike. That is, changes in NTD rearrangements can not only

286 directly affect the RBD motion of neighboring protomers, but also influence the glycans at the

287 interface of these two critical domains. These differentially oriented glycans can aid in maintaining

288 altered RBD conformations between variants.

289

290 **RBD-gating motion is allosterically modulated by the adjacent NTD**

291 There has been a putative conjecture that the structure and dynamics of the NTD may be

292 allosterically connected to RBD gating[40, 57]. Given the distinctive RBD and NTD rotational

293 conformations observed above and the notable reorientation of key glycans between these two

294 critical domains (cf. **Figs. 3, 4, 5**), we set out to study the cross-correlated fluctuations that may

295 drive large-scale allosteric motions within the peplomer. The inter-residue dynamic cross-

296 correlation plots (**Figs. S9, S10**) indicate that beyond the expected strong correlations within

297 individual NTD and RBD domains, there is a remarkable inter-domain NTD-RBD synchronization

298 of dynamics as well. One must note that in the closed conformation, the RBD of one protomer

299 directly interacts with the NTD of the protomer situated anti-clockwise to it (cf. **Fig. 1a**). In our

300 findings, as seen in **Figs. S9a/b,** the RBD of chain A is correlated with the NTD of chain B, the

301 RBD of chain B is correlated with the NTD of chain C, and the RBD of chain C is correlated with

302 the NTD of chain A in both G614 and Delta closed conformations. More remarkably, the up-RBD

303   (chain B), even in the open conformation, has strongly correlated fluctuations with the neighboring

304   NTD (chain C), which is much stronger in the Delta variant as compared to G614 (**Fig. 6a/b**).

305   Once the RBD moves up, it is no longer in direct interaction with any neighboring domain. Yet

306   this strong correlation of motion suggests allosteric communication between the up-RBD and the

307   NTD to its right. Recollecting the role of glycans N165 and N234 from that NTD and N331 from

308   the base of the up-RBD in propping the receptor binding domain in distinct conformations (Fig.

309   5), these glycans may be the key to NTD-RBD cross-talk over and above communications via the

310   protein backbone. This strong correlated motion between inter-protomer NTD and RBD in the up-

311   conformation and its relative increase in strength in Delta establishes the critical role of NTD in

312   RBD gating and indicates that this allosteric communication is better optimized in the Delta

313   variant.

314   To extract the large-amplitude low-frequency dynamics that result from these correlated

315   fluctuations, we performed a Principal Component Analysis (PCA) over the simulated ensemble

316   (see details in SI Methods). We extracted the top two PCs that maximize the variance in motions

317   and that define the majority of the essential dynamics that drive Spike equilibrium motions. These

318   PCs in both up and down conformations indicate that in equilibrium conditions, the dominant

319   motions are mainly confined at the bulk-head of the Spike, within the NTD-RBD regions – at least

320   within the microsecond time-scale sampled in our simulations (**Fig. S11**). Let us independently

321   consider the down and up configurations of the Spike. With all RBD down and closed, there is a

322   distinct separation in RBD-NTD orientation between G614 and Delta variants (Fig. **S9 c/d**) along

323   PC1. The RBD is rotated closer to the central axis in Delta, with a concomitant rotation of the

324   neighboring NTD inward towards the RBD. The PC2 motion remains invariant between G614 and

325   Delta, indicating that NTD-RBD correlated allostery has a variant-independent component.

326   Looking at the up-conformations next (**Fig. 6c**), we find a similar variant independent NTD-RBD

327   allosteric component, which forms the essential motion with the highest contribution (i.e., along

328   PC1). PC2, however, shows a significantly high occurrence of separation between G614 and Delta,

329   where the up-RBD is tilted more inwards towards the central axis in Delta, accompanied by the

330   NTD tilted downward towards the stem of the Spike (**Fig. 6d**). This correlated motion is similar

331   to the combination of RBD and NTD orientational variations discussed above (cf. **Figs. 3, 4**),

332   establishing that the RBD opening-twisting motion and the NTD tilting motion are allosterically

333   coupled, further implicating the role of NTD in Spike gating.

334

D950N Mutation in Delta Alters HR1 Dynamics and Spike Stability

336

337   Beyond the RBD mutations that are expected to have direct ACE2 binding and antibody

338   escape effects[37], the FCS mutation with furin cleavage effect[58], and the other varied

339   NTD/RBD mutation effects as discussed above, the Delta variant also has the interesting D950N

340   substitution. This is structurally located in the S1-S2 interface and at the highly conserved heptad

341   repeat (HR1) (cf. Fig. 1). To shed light on the evolutionary advantage of having this mutation on

342   an otherwise conserved helix, we performed a detailed structural analysis of this region. To

343   elucidate the impact of D950N, it is instructive to identify any residues that interact with the

344   mutation site 950. For this, we calculated the probability of contacting residue 950 for all other

345   residues in the Spike, using the G614 and Delta simulations (**Fig. S12**). We find only two residues

346   (i.e. E309 and R1014; see **Fig. S12**) that form noticeable contacts with 950, in both the G614 and

347   Delta systems. Because these residues are negatively (E309) and positively (R1014) charged, their

348   interactions with 950 are expected to alter since the D950N mutation removes the negative charge.

349   To discern possible changes in these interactions, we calculated distances between (i) 950 and 309,

350   and (ii) 950 and 1014, for G615 (with D950) versus Delta (with D950N). The results indicate that

351   the D950N mutation leads to distinct distance distributions, especially when comparing the up-

352   protomers of G614 against Delta (**Figs. S13, S14**). These changes suggest that the HR1 may

353   undergo variant-specific fluctuations.

354   To properly capture the dynamics of HR1, we note that the HR1 consists of two helices as

355   shown in **Fig. 7a and 7b**, which are in the regions ~910-941 (referred to as "HR1-bottom") and

356   ~942-986 ("HR1-top"). Since HR1-bottom and HR1-top may undergo independent

357   rearrangements from each other, we define separate sets of coordinates that describe the movement

358   of each part individually. That is, for each HR1 part, we introduced a tilting and a torsion

359   coordinate, which are measured relative to the central helix (CH) of the Spike (see SI for details;

360   **Figs. S15-S18**). For the HR1-top region (which has the mutation site D950N), the most noticeable

361   difference between G614 and Delta is in the fluctuation along the torsion coordinate, in the up-

362   protomer (**Fig. S15, S16**). Specifically, HR1-top of G614 exhibits a larger range of torsion angles

363   in the up-protomers, while the torsion range in the remaining down-protomers is smaller. In

364   contrast, the torsion range of the HR1-top in Delta remains smaller in all protomers, regardless of

365   up or down (**Fig. S15, S16**). For the HR1-bottom region, the most dominant difference between

366 G614 and Delta is in the rearrangement along the tilting coordinate, in the up-protomer (**Fig. S17**).

367 Specifically, the HR1-bottom of the up-protomer in Delta can reach significantly larger tilting

368 angles (max tilt ~30°), compared to the G614 simulations (maximum tilt ~20°).

369 Together, the analyses of **Figs. S15-S18** allow us to identify the relevant motions of each

370 HR1 part, along which changes between the variants occur. To summarize these changes, we plot

371 2D distributions along (a) the torsion of the HR1-top and (b) the tilt of the HR1-bottom, which

372 encapsulate the key differences between the G614 and Delta simulations (**Fig. 7**). In conclusion,

373 the results demonstrate that, specifically for an up-protomer, the D950N mutation can be

374 responsible for complex changes in HR1 rearrangements (**Fig. 7**), which may influence how

375 glycans shield this region as discussed below (cf. **Fig. 8**), or even influence Spike-host fusion

376 events.

377
378 **Glycan Shielding of the Fusion Peptide and HR1 is Enhanced in Delta**
379
380 The fusion peptide (FP) region consists of sequences (800-860) that are highly conserved

381 and are a hotbed of broadly neutralizing antibody targets and vaccine-design efforts[44, 59]. While

382 the sequences in the FP region are conserved, mutations from other parts of the Spike can alter the

383 shape, fluctuation, or glycan shielding of the FP region. A detailed understanding of these aspects

384 would enable future experiments to develop more precise therapeutics.

385 Since glycan shielding is a critical factor for antibody evasion, we have identified which

386 glycans are responsible for shielding the FP region. We have also examined if and how the glycan

387 shielding may change (i) for different variants (i.e. G614 vs. Delta) and (ii) for different protomer

388 conformations (i.e. all-down vs. 1-up). For the 800-860 region, we calculated the glycan coverage

389 for the all-down G614, all-down Delta, 1-up G614, and 1-up Delta simulations (**Fig. S19a-d**). For

390 all four simulation systems, glycans 603, 283, and 709 are the dominant contributors to shielding

391 the FP. To quantify the extent of glycan shielding, we calculated the glycan-encounter-factor

392 (GEF)[47] for each residue of this region (**Fig. S19e/f**). Overall, residues 805-825 receive on

393 average less glycan shielding, while 800-803 and 830-855 receive greater shielding. Interestingly,

394 this GEF profile remains similar across different protomer conformations, as well as variants (**Fig.**

395 **S19e/f**). Hence, these findings suggest that glycan shielding of the FP region is a robust feature of

396 Spike function, with glycans 603, 283, and 709 being the key contributors.

13

397   Given the cross-reactive human monoclonal antibody response found to be mounted over

398   different sarbecovirus Spikes at the HR1 domain[45, 46], and the Delta-specific D950N mutation

399   and causing dynamic variations in this neighborhood, we also performed a similar glycan coverage

400   analysis for the 915-940 region (**Fig. 8**). All four simulation systems (i.e. all-down G614/Delta

401   and 1-up G614/Delta) indicate that glycans 603, 801, and 1098 are the dominant contributors to

402   shielding the 915-940 region (**Fig. 8a-d**). As for quantifying the extent of glycan shielding, the

403   GEF profile is overall similar between the all-down G614 and all-down Delta simulations (**Fig.**

404   **8e**). Specifically, in each down-protomer of either variant (**Fig. 8e**), residues 915-925 receive

405   overall greater glycan shielding, while residues 930-940 exhibited lower glycan shielding.

406   Interestingly, this GEF profile remains overall similar in the up-protomer of the 1-up G614

407   simulations (**Fig. 8f**). However, the GEF profile changes significantly in the up-protomer of the 1-

408   up Delta simulations. Specifically, the glycan coverage around residues 925-935 is noticeably

409   higher in the up-protomer of Delta, as compared to the G614 variant (**Fig. 8f**). In summary, the

410   glycan shielding of the 915-940 region in the G614 variant is independent of protomer

411   conformation (cf. **Fig. 8e/f**). By contrast, glycan shielding increases for the Delta variant if the

412   protomer is in the up-RBD conformation (cf. **Fig. 8e/f**). In particular, this increased shielding is

413   attributed to the contributions from glycans 801 and 1098 in the up-protomer state, while the

414   contribution from glycan 603 remains effectively constant between protomer conformations.

415

DISCUSSION

417

418   Being exposed on the surface of the virus and forming the first line of contact with the host,

419   different modalities of vaccine design, immune-mediated therapeutics, and even many small-

420   molecule drugs primarily revolve around the SARS Spike glycoprotein. A molecular-level

421   understanding of the mechanism of immune evasion, as well as the dynamic cascade of events that

422   lead to functional interaction with the ACE2 receptor, is needed to get a better understanding of

423   this critical protein. However, due to structural complexities, as well as constantly evolving

424   antigenic surfaces, the structure-dynamic relationships of this glycoprotein are not easily attainable

425   through experimental studies. As utilized here, a computational approach provides strong

426   alternatives to augment experimental findings. Even though the SARS-CoV-2 virus has shown an

427   impressive number of variants accumulating over time from its emergence in late 2019, the D614G

428   substitution was one early natural selection[29] that has stably persisted through subsequent

429   evolutionary events. On the other hand, the Delta variant emerged as one of the most virulent, with

430   high symptom severity among the VOCs[9]. The Delta variant serves as an ideal model for

431   studying the interplay between infectivity, immune evasion, and structural adaptability. Many of

432   the key mutational effects observed in Delta remain relevant, as similar alterations persist in

433   Omicron-derived sublineages[60] and later variants. Additionally, immune escape mechanisms

434   first observed in Delta shaped the trajectory of SARS-CoV-2 evolution, reinforcing its role as a

435   valuable reference for future studies on viral adaptation and immunogen design[61]. Here, to

436   illustrate allosteric coupling mechanisms and antibody evasion strategies that provide fitness

437   advantages to a specific variant, we perform a comparative examination of the D614G and Delta

438   (B.1.617.2) Spike dynamics , as well as quantify the intrinsic Spike properties that have remained

439   invariant despite evolution.

440   Of the ~22 glycans present on an individual Spike protomer, nine are present on the NTD,

441   one on the RBD, and one on the connector between these two domains. Like most peplomeric

442   glycans, one of their primary purposes is shielding the underlying antigenic surface from antibody

443   interaction. The Spike NTD houses the epitopes of several broadly neutralizing antibodies,

444   instigating a repertoire of mutations and deletions, many of them within the residue ranges of 14-

445   26, 141-156, and 246-260, commonly known as the NTD supersite due to their high antibody

446   sensitivities[49]. This study demonstrates that the NTD glycans, specifically N17, N149, N165,

447   N234, and N282, are reorganized in their spatial orientation, possibly through the 5 Delta

448   mutations and two deletions in this domain (see **Fig. 1b**). Consequently, the shielding effect

449   increases over the Delta NTD, especially around the supersite residues (**Fig. 2, S1**). This explains

450   the reduced neutralization capability of NTD-specific antibodies to the Delta[50, 51], allowing this

451   variant to evolve into a more immune-evasive variety. While most studies target the direct local

452   interactions of the substituted amino acids with antibodies to explain changing immune responses,

453   this finding shows that it is essential to take the local glycan orientation into account as well.

454   The upward gating of the RBD is an essential dynamic transition that causes ACE2 binding

455   and subsequent fusion events. However, the RBD-open conformation also allows for antibody

456   targeting that competes with the host receptor. Our findings establish that the Delta RBD, on

457   average, adopts a less erect poise, having lower 'opening' and 'twisting' angles as compared to

458   the G614 RBD (**Fig. 3**). From our analysis, it is evident that this structural basin concedes greater

459   steric clearance from neighboring domains (**Fig. S6**), allowing for multiple RBDs to open
460   simultaneously, which has already been evidenced in experiments[62]. This greater separation
461   between neighboring up-RBDs also justifies the hitherto unexplained multiple ACE-2 associations
462   observed in Delta without expected steric clashes[24]. We speculate that this differently poised
463   up-RBD probability may also aid in avoiding receptor binding motif targeting antibodies while
464   allowing for multi-valent ACE2 interactions.

465   Complementing the differential stance of up-RBD, our results also illuminate a differently
466   oriented NTD with a higher probability of being more tilted towards the Spike stem (**Fig. 4**) in
467   Delta. We speculate that the multiple amino acid substitutions and deletions alter the local
468   structural arrangements in the NTD, which in turn affects the dynamics of this domain, making it
469   take up an altered tilt, as well as reorient the NTD glycans and consequent shielding, as discussed
470   before. The exact role of the large globular NTD in the Spike function has been elusive. Many
471   antibodies have been found to target the NTD, rather than the ACE2-binding motif, yet it is unclear
472   how binding to this distant domain results in Spike neutralization[13]. This indicates that
473   preventing the normal dynamics of the NTD with the bulky attachment of antibodies somehow
474   arrests the downstream functioning of the Spike. Keeping in mind that the RBD of one protomer
475   is in physical interaction with the neighboring protomer NTD (situated anticlockwise, to the right),
476   our conjecture is that the tilting and torsional motion sampled by the NTD dynamics (**Fig. 4**)
477   triggers RBD opening in the directly neighboring protomer.

478   Another noteworthy finding has been the effects of a trifecta of glycans around the open
479   RBD (in protomer B). Glycans N165 and N234 from the adjacent NTD (in protomer C) and glycan
480   N331 from the base of the up-RBD have altered orientations in terms of overall sampled space
481   (**Fig. 5**). It has been previously understood that beyond shielding, glycans also aid with RBD
482   transitions[42]. Here, we further demonstrate that the glycans also play vital roles in locking the
483   RBD in specific positions by nudging against the RBD base. These interfacial glycans not only
484   help with optimized glycan shielding but also influence the RBD conformations by helping the
485   domain maintain varied structural stances – in the case of Delta, allowing for a more bent
486   conformation towards the central Spike axis.

487   Given the NTD and RBD dynamics sample altered landscapes for G614 and Delta Spikes,
488   and that glycans can reorient and affect domain dynamics between these variants, we have also
489   elucidated the correlated motions and large-amplitude essential dynamics captured in the

490   simulations. Our findings validate that the NTD and RBD demonstrate the largest motions along

491   the high-contribution variational coordinates. Moreover, beyond the intra-domain correlations, the

492   inter-protomer NTD and RBD show strongly correlated motions. Most noteworthy is the coupling

493   between the up-RBD and the neighboring NTD (anti-clockwise) that becomes stronger for Delta.

494   This validates our conjecture that the motions of the NTD may trigger the adjacent RBD dynamics.

495   PCA demonstrates that both closed and open Spikes tend to occupy separate RBD-NTD relative

496   orientation and rotational conformations between the two variants (**Fig. 6, S9**). These different

497   orientations, also captured by our reaction coordinate analyses (cf. **Fig. 3, 4**), are strongly coupled,

498   as evidenced by the high eigenvalues of the PCA. Yet, one of the top two eigenvalue components

499   (PC1 for down-RBD and PC2 for up-RBD) is variant-independent. These motions, therefore,

500   extract the invariant allosteric signaling between NTD and RBD that is intrinsic to the Spike

501   functioning – demonstrating the dynamic role of NTD in the RBD gating action.

502   Similar mutation-induced allosteric alterations are also possible in other regions of Spike

503   as highlighted by another vital mutation of the Delta that is interestingly situated away from the

504   RBD or NTD, which is the D950N substitution on the otherwise conserved HR1 helix. Our

505   simulations demonstrate the D to N substitution in this position, which removes a negative charge,

506   affects the local electrostatic interactions with E309 and R1014. As a result, the HR1 dynamics is

507   altered significantly (**Fig. 7**), with the top half of the HR1 region having greater torsional motion

508   in G614 and the bottom half having a greater tilting motion in Delta. These dynamic changes

509   affected the exposure of the HR1 epitope region, where the glycan shielding is increased in the

510   Delta RBD-up conformation. Located at the interface of S1/S2, these dynamic variations can also

511   influence fusion with the host membrane, possibly enhancing the fusion ability in Delta[62].

512   In summary, this study has elucidated the allosteric modulation of Spike RBD by the N-

513   terminal domain of the neighboring protomer. This dynamic coupling has both a variant-dependent

514   and an invariant component. Delta-specific mutations on the NTD cause local structural changes

515   that affect the rotation and tilting of the NTD. This has two important consequences critical to

516   Spike's behavior. The glycans on the NTD get differently oriented and cause greater antigenic

517   surface shielding, rendering the Delta variant less sensitive to NTD-specific antibody

518   neutralization. Secondly, this altered rotational dynamics of the NTD is allosterically

519   communicated to the neighboring RBD, causing it to, in turn, sample a modified twist and opening

520   conformation. A trio of glycans engages the RBD in this changed conformation, which allows for

17

521   reduced steric clash and multiple RBD-open modes. A cryo-EM study has demonstrated that the

522   Delta Spike exhibits extensive diversity in open-close substates compared to other variants [52]

523   Besides the mutation-dependent RBD-NTD communications, there are variant-independent

524   allosteric dynamics that lead the NTD bulk-head motions to trigger the RBD-gating mechanism

525   under equilibrium conditions, without external forces. The D950N mutation at the HR1 further

526   affects the S2 helix dynamics, governing the glycan coverage in the HR1 epitope region.

527   The antigenic nature of the Spike, along with its critical functional aspects of receptor

528   binding, as well as the plasticity of multiple conformations, make this protein an attractive target

529   for drug and vaccine development studies targeting potential human coronaviruses. When properly

530   understood, its functional versatility and complexity can be harnessed to understand evolutionary

531   strategies of other coronaviruses. With control over variant-specific structural coupling (e.g.

532   differential NTD-RBD relative orientations) and glycan coverage (e.g. over NTD supersite and the

533   conserved HR1) as well as the invariant allostery (e.g. NTD-triggered RBD gating) and epitope

534   shielding (e.g. over the flexible fusion peptide region), both VOC-specific as well as generalized

535   sarbecovirus immunogen strategies can be engineered. Targeting allosteric pathways that regulate

536   RBD gating—rather than just the ACE2-binding interface—could be a promising avenue for

537   designing broadly effective inhibitors. Additionally, understanding glycan shielding at the NTD

538   and HR1 regions provides a rationale for optimizing monoclonal antibody cocktails that account

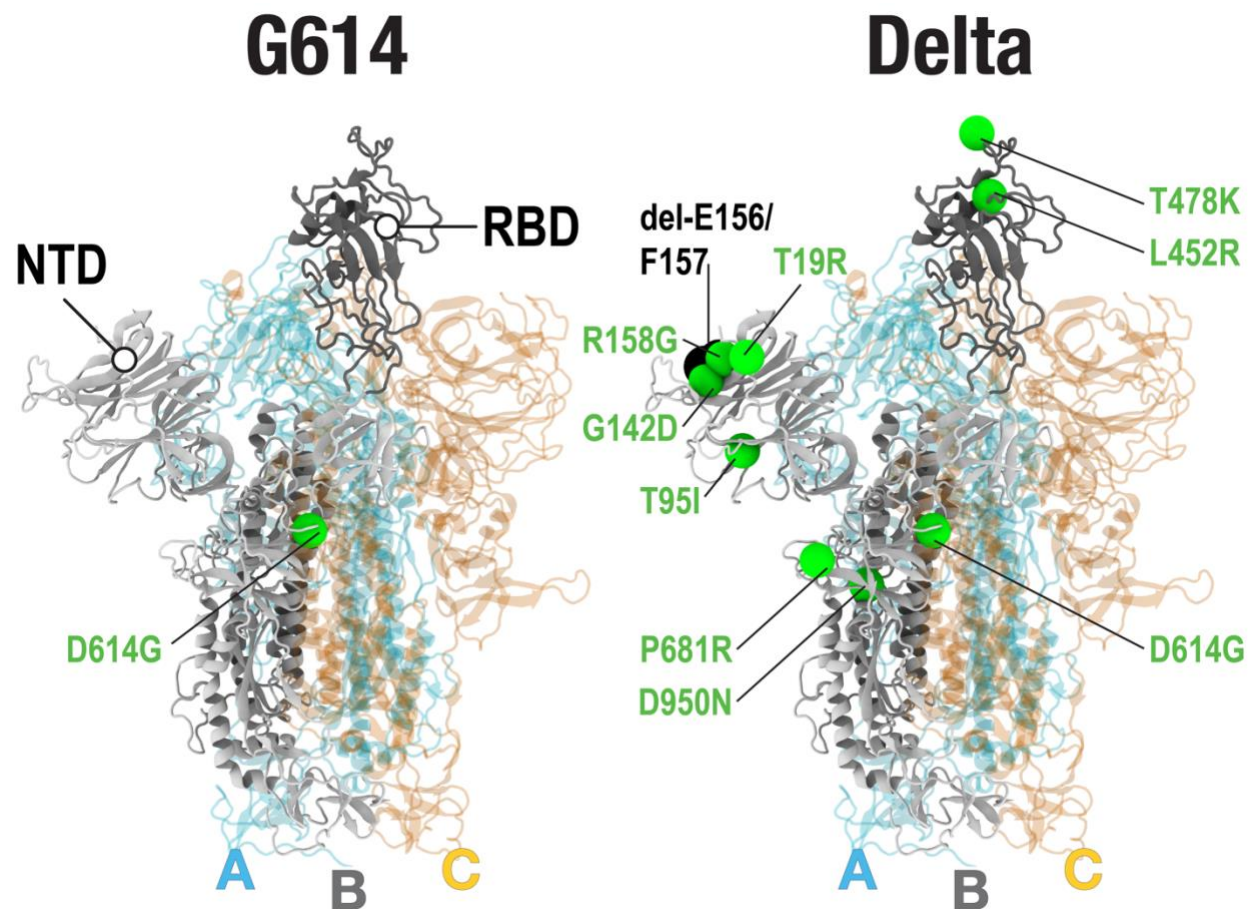539   for glycan-induced epitope occlusion.

540

541   **FIGURES**
542
543

544
545
546
547   **Figure 1. Structural description of the Spike protein, with the mutation/deletion sites that**
548   **define the G614 and Delta variants.** Point mutations are represented by green beads, and residue
549   deletions by black beads. (Left) Depiction of the G614 Spike variant with the D614G mutation.
550   (Right) Depiction of the Delta Spike variant. The NTD of Delta contains four mutations (T19R,
551   T95I, G142D, and R158G), and two deletions (del-E156 and del-F157). The RBD of Delta harbors
552   two mutations, L452R and T478K. Additional mutations in Delta are D614G, P681R, and D950N.
553   In each Spike, the protomers "A, B and C" are colored cyan, gray and orange, respectively. In each
554   spike, the RBD of protomer B is in the up conformation, while the RBDs of protomers A and C
555   are in the down conformation. All molecular images were created using VMD[63].
556
557
558
559

19
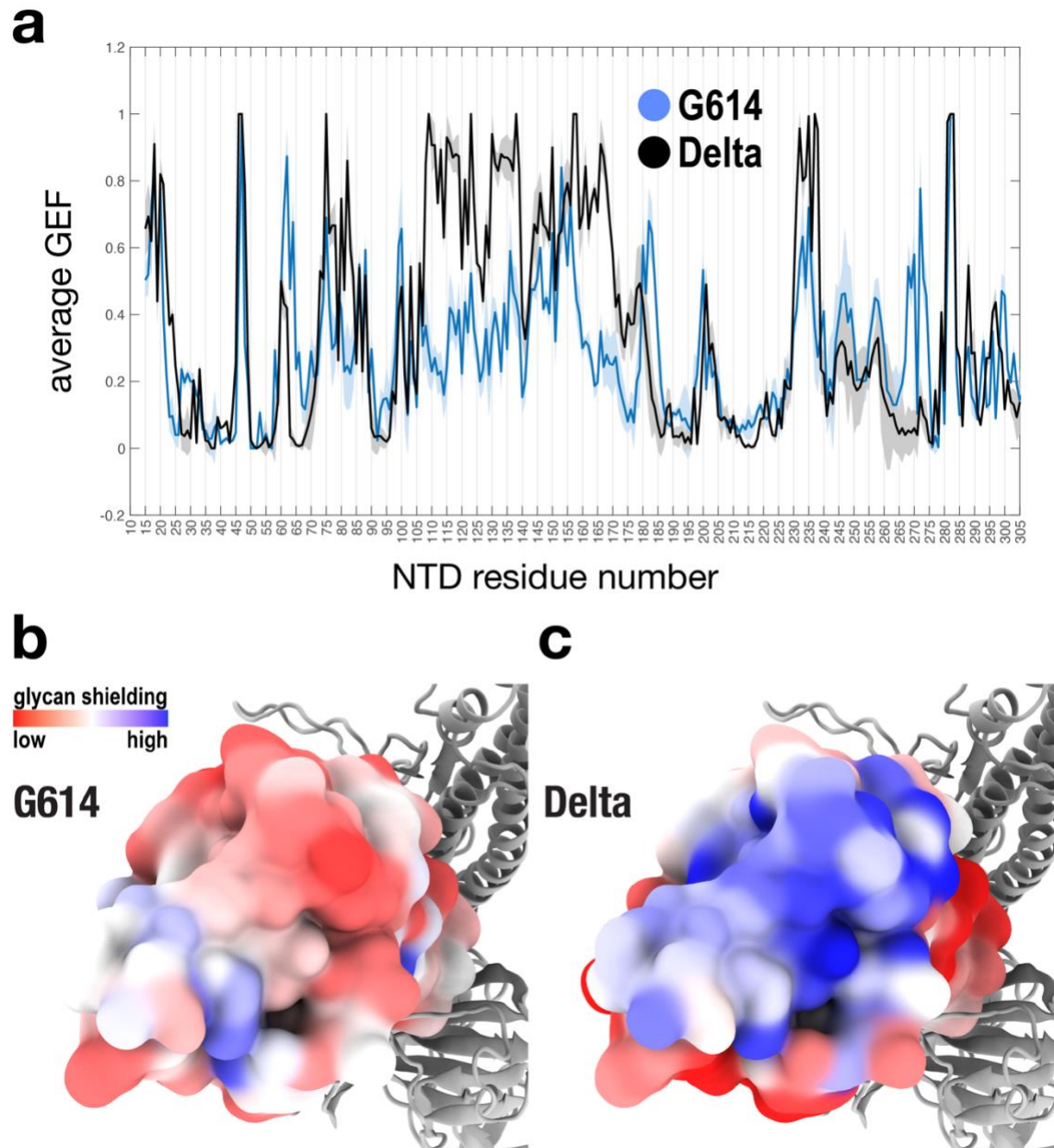
Figure 2. Glycan shielding of NTD surface. (**a**) To quantify glycan shielding, we calculated the glycan encounter factor (GEF) as function of NTD residue, for the G614 (blue) and Delta (black) simulations. The blue and black solid lines represent averages from all three protomers of the all-down G614 and all-down Delta systems, respectively. Filled error-bar envelopes show standard deviations. (**b/c**) To provide a structural interpretation, the average GEF values (as shown in panel **a**) are mapped onto NTD for (**b**) the G614 and (**c**) Delta variant. Qualitatively, GEF values are shown from low shielding (red) to high shielding(blue).

20
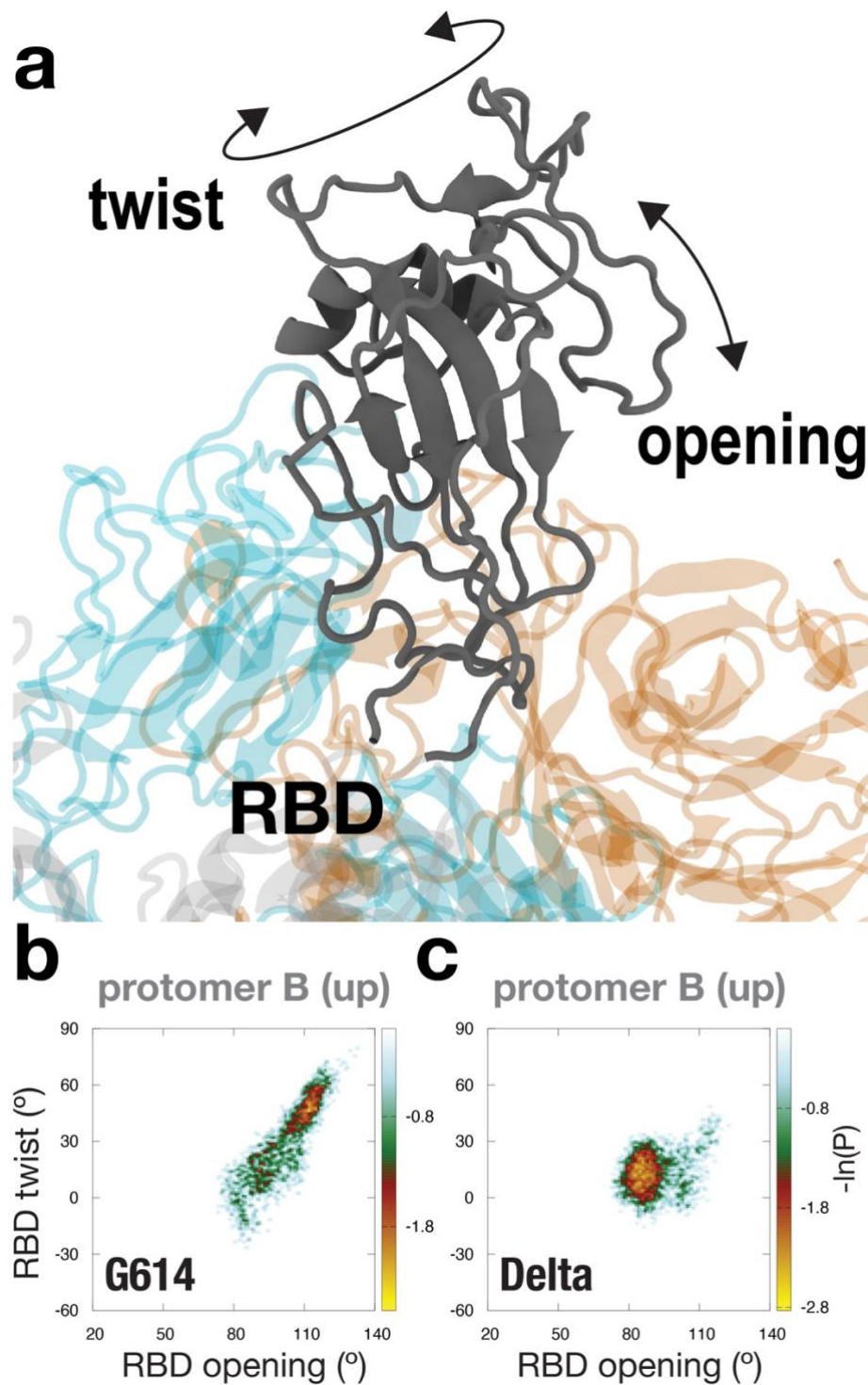
Figure 3. Movement of the up-RBD in protomer B, for 1-up G614 versus 1-up Delta. (**a**) To describe RBD rearrangements, we defined opening and twisting coordinates for RBD (see SI Methods for details). The up-RBD region is a zoomed-in view from **Fig. 1a**. (**b/c**) 2D distributions along RBD opening and RBD twist. The distributions in (**b**) and (**c**) describe the motions of the up-RBD in protomer B for the (**b**) 1-up G614 and (**c**) 1-up Delta systems, respectively.
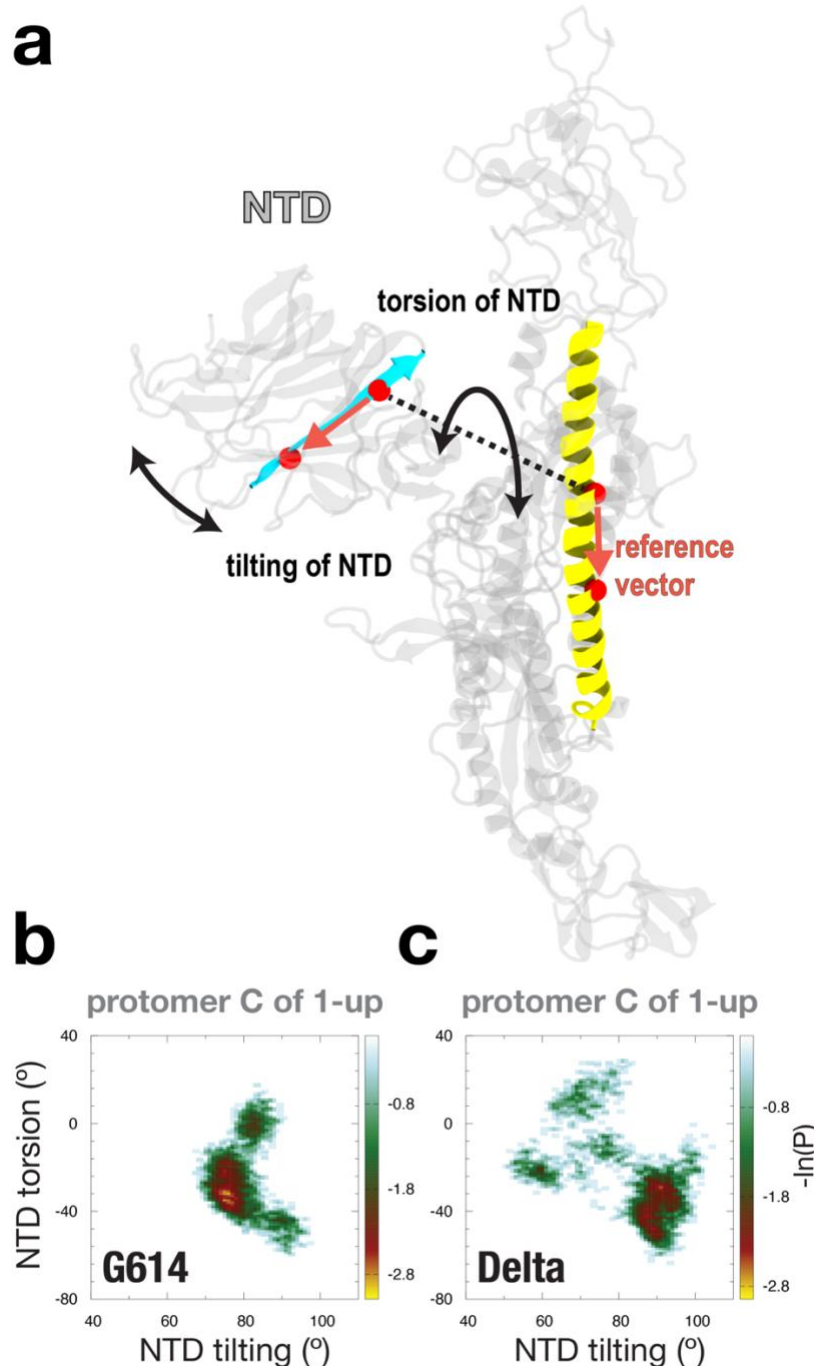
21

Figure 4. Movement of NTD in protomer C, for 1-up G614 versus 1-up Delta. (**a**) To describe NTD rearrangements, we defined tilting and torsion coordinates for NTD (see SI Methods for details). (**b/c**) 2D distributions along NTD tilting and NTD torsion. The distributions in (**b**) and (**c**) describe the motions of the NTD in protomer C for the (**b**) 1-up G614 and (**c**) 1-up Delta systems, respectively. Note that the NTD of protomer C is adjacent to the up-RBD of protomer B. Therefore, panels (**c**) and (**b**) are shown here to illustrate how the orientation of the protomer-C NTD may influence the orientation of the protomer-B RBD (cf. **Fig. 3**).
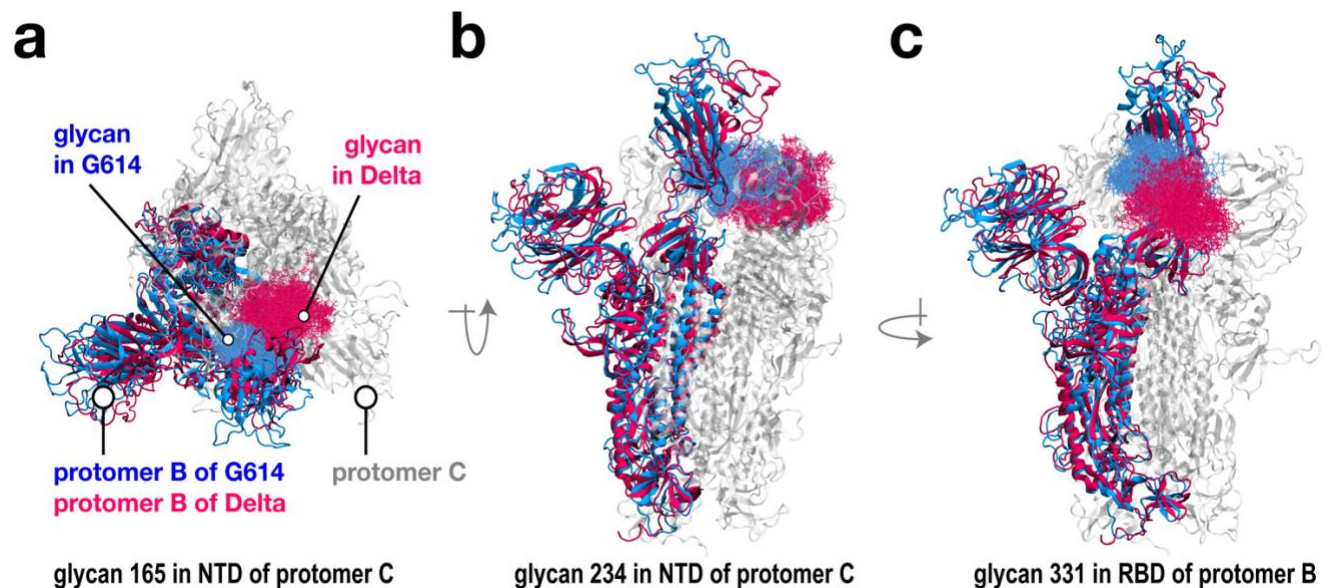
22

589
590

glycan 165 in NTD of protomer C   glycan 234 in NTD of protomer C   glycan 331 in RBD of protomer B

591
592
593
594 **Figure 5. Distinct glycan positioning in G614 versus Delta may lead to distinct up-RBD**
595 **orientations.** Near the up-RBD of protomer B, the simulations suggest that glycans (**a**) 165 and
596 (**b**) 234 in the NTD of the neighboring protomer C, and (**c**) glycan 331 in the RBD of protomer B
597 adopt distinct orientations in the G614 (blue) versus Delta (magenta) simulations. In all panels, the
598 overlayed blue and magenta structures are representative conformations of protomer B from the
599 dominant up-RBD basins of the G614 (i.e. blue) and Delta (i.e. magenta) simulations, respectively
600 (cf. **Fig. 3b/c**). In each panel, the neighboring protomer C is shown in orange, for reference. In
601 panels **a/b/c**, blue point densities depict the positions of glycans (**a**) 165, (**b**) 234, and (**c**) 331 in
602 the G614 simulations. Similarly, magenta point densities depict the positions of glycans (**a**) 165,
603 (**b**) 234, and (**c**) 331 in the Delta simulations.
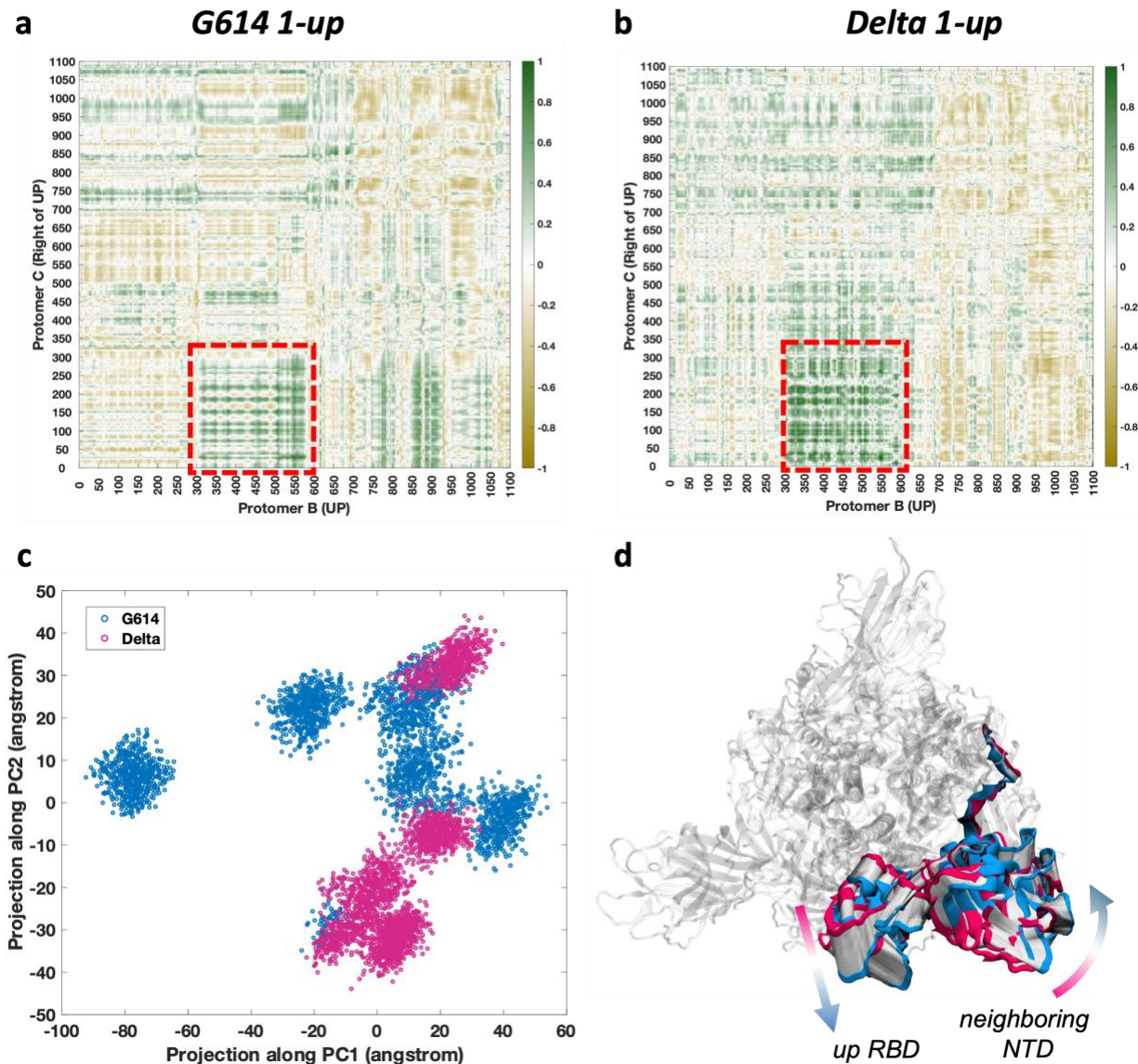604
605
606
607
608
609

23

Figure 6: Differences in correlated motion of up-RBD with neighboring NTD, between G614 and Delta. (**a**) Inter-residue cross-correlation of RMS fluctuations between protomer B (RBD-up) and Protomer C (right neighbor) in G614 (1-up), and (**b**) Delta (1-up) conformations. Interprotomer RBD-NTD correlation space is indicated by red box. (**c**) Projection of the G614 (blue) and Delta (magenta) ensembles along the top two principal component eigenvectors. PC analysis was performed over the two combined ensembles to extract the variances in large-amplitude motions (see methods for details). (**d**) Structural representation of motion along PC2, which describes the dominant difference in motion between G614 and Delta. Magenta structure represents negative PC2 (Delta-like) and blue represents positive PC2 (G614-like), with interpolation given in white. Motion of the up-RBD (protomer B) and neighboring NTD (protomer C) is shown here.
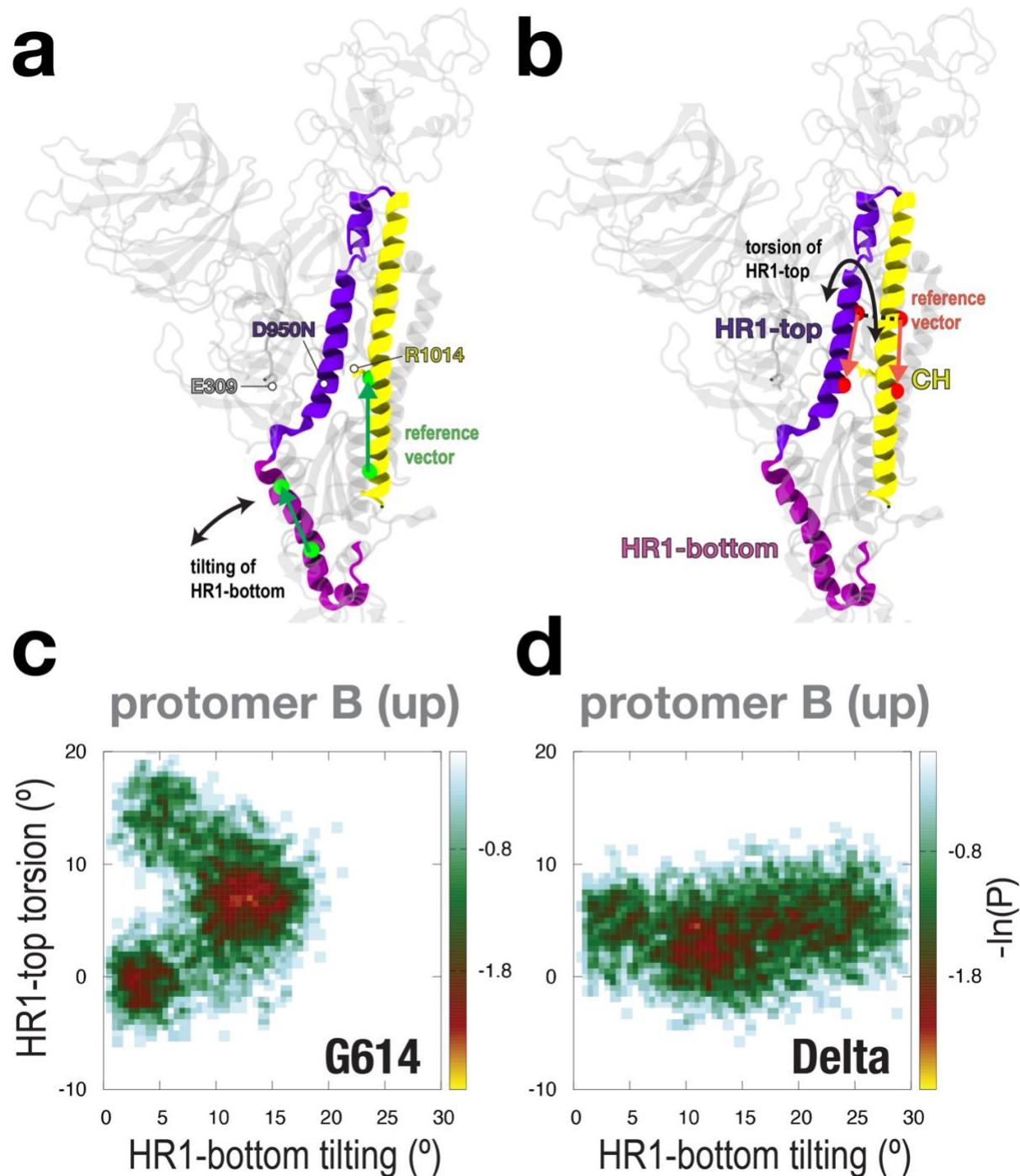
24

Figure 7. Movement of HR1 in protomer B, for 1-up G614 versus 1-up Delta. (**a/b**) To describe HR1 rearrangements, we capture motions in the bottom (purple) and top (violet) part of HR1. Specifically, we measure (a) a tilt of HR1-bottom relative to CH (yellow) and (b) a torsion of HR1-top relative to CH. See **Figs. S15** and **S17** for details on how these coordinates are defined. (**c/d**) 2D distributions along HR1-bottom tilting and HR1-top torsion. The distributions in (**c**) and (**d**) describe the motions of the HR1 in protomer B for the (**c**) 1-up G614 and (**d**) 1-up Delta systems, respectively.
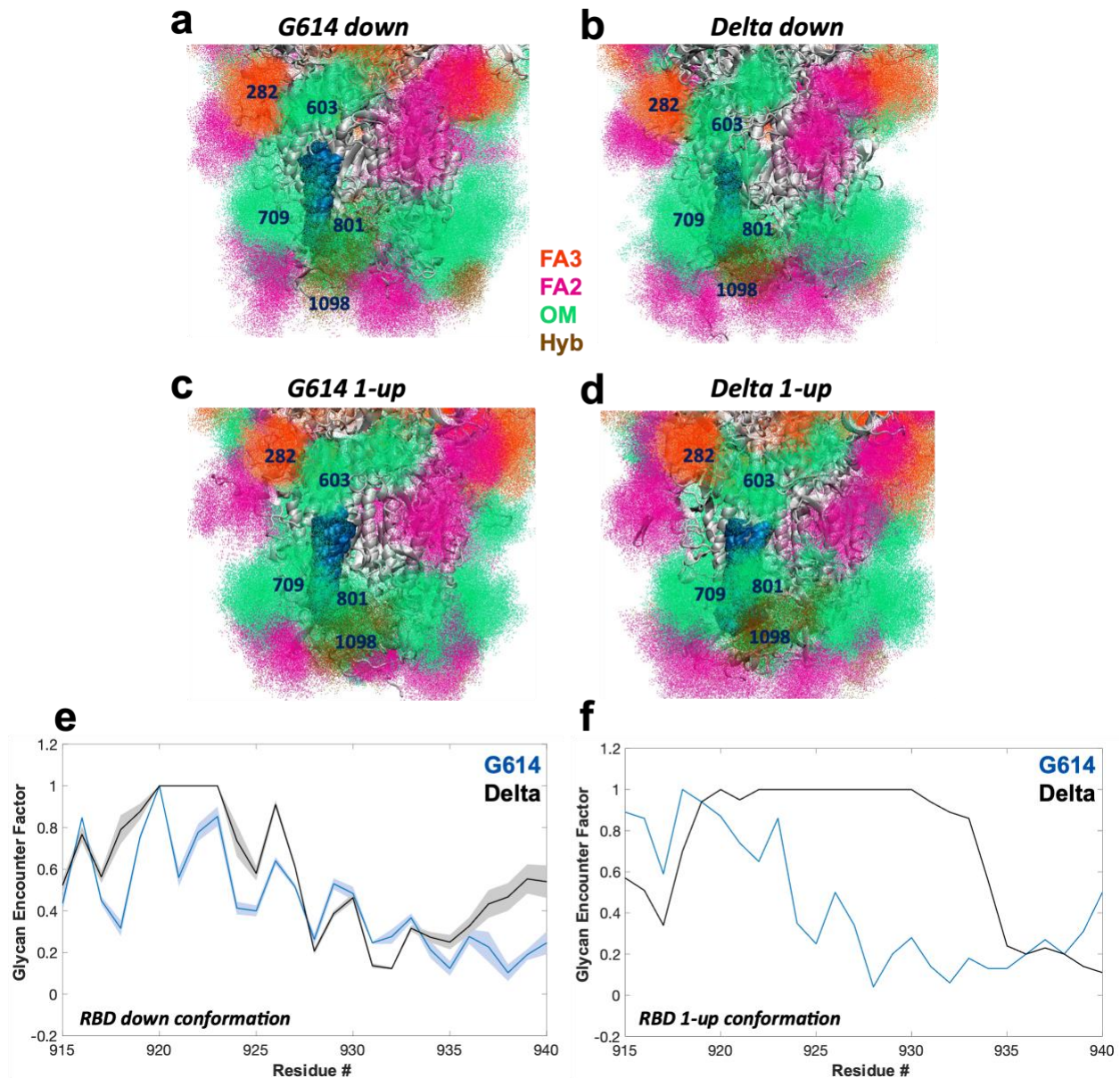
25

634

Figure 8. Glycan shielding of the HR1 epitope (residues 915-940) region.
(**a**) G614 all-down, (**b**) Delta all-down, (**c**) G614 1-up, and (**d**) Delta 1-up conformations of the fusion peptide region. Multiple conformations of the fusion-peptide residues 800 to 860 are shown in dark blue, and the rest of the protein is shown in gray. Glycans near this region are represented by density of points, and colored according to the labeling. (**e**) Residue-wise GEF plot for G614 (blue) and Delta (black) Spikes in the RBD down conformation. Mean GEF values from the three protomers are shown, with standard deviation. (**f**) Residue-wise GEF plot for G614 (blue) and Delta (black) Spikes in the RBD 1-up conformation. GEF values only from the up protomer are shown.

26

656

657 **Author contributions:** S.C., K.N., and S.G. conceptualized the study and designed the
658 experiments. S.C. and K.N. prepared the structures. SC ran the simulations. S.C., K.N., and S.G.
659 performed the data analysis and interpretation. S.C. and K.N. prepared the figures. S.C., K.N.,
660 M.Z, and S.G. wrote and edited the manuscript. S.C. and S.G. are co-corresponding authors.

661

662 **Competing interests:** The authors declare no competing interests.

663 **Data and materials availability:** Data and materials are available from the corresponding
664 authors upon request.

665

666

667

668

669

670 **REFERENCES**

671

672 1. Sanjuan, R. and P. Domingo-Calap, *Mechanisms of viral mutation.* Cell Mol Life Sci,
673 2016. **73**(23): p. 4433-4448.
674 2. Duffy, S., *Why are RNA virus mutation rates so damn high?* PLoS Biol, 2018. **16**(8): p.
675 e3000003.
676 3. Organization, W.H., *COVID-19 weekly epidemiological update, edition 115, 26*
677 *October 2022.* 2022. https://www.who.int/publications/m/item/weekly-
678 epidemiological-update-on-covid-19---26-october-2022.
679 4. Organization, W.H., *Tracking SARS-CoV-2 variants, 28 October 2022.* 2022.
680 https://www.who.int/activities/tracking-SARS-CoV-2-variants.
681 5. Balint, G., B. Voros-Horvath, and A. Szechenyi, *Omicron: increased transmissibility*
682 *and decreased pathogenicity.* Signal Transduct Target Ther, 2022. **7**(1): p. 151.
683 6. Aleem, A., A.B. Akbar Samad, and A.K. Slenker, *Emerging Variants of SARS-CoV-2*
684 *And Novel Therapeutics Against Coronavirus (COVID-19)*, in *StatPearls*. 2022:
685 Treasure Island (FL).
686 7. Antonelli, M., et al., *Risk of long COVID associated with delta versus omicron*
687 *variants of SARS-CoV-2.* Lancet, 2022. **399**(10343): p. 2263-2264.

688 8.   Bager, P., et al., *Risk of hospitalisation associated with infection with SARS-CoV-2*
689   *omicron variant versus delta variant in Denmark: an observational cohort study.*
690   Lancet Infect Dis, 2022. **22**(7): p. 967-976.
691 9.   Patrick, C., et al., *Biophysical Fitness Landscape of the SARS-CoV-2 Delta Variant*
692   *Receptor Binding Domain.* J Mol Biol, 2022. **434**(13): p. 167622.
693 10.   Jackson, C.B., et al., *Mechanisms of SARS-CoV-2 entry into cells.* Nat Rev Mol Cell
694   Biol, 2022. **23**(1): p. 3-20.
695 11.   Harvey, W.T., et al., *SARS-CoV-2 variants, spike mutations and immune escape.* Nat
696   Rev Microbiol, 2021. **19**(7): p. 409-424.
697 12.   Amanat, F., et al., *SARS-CoV-2 mRNA vaccination induces functionally diverse*
698   *antibodies to NTD, RBD, and S2.* Cell, 2021. **184**(15): p. 3936-3948 e10.
699 13.   Liu, L., et al., *Potent neutralizing antibodies against multiple epitopes on SARS-CoV-2*
700   *spike.* Nature, 2020. **584**(7821): p. 450-456.
701 14.   Walls, A.C., et al., *Structure, Function, and Antigenicity of the SARS-CoV-2 Spike*
702   *Glycoprotein.* Cell, 2020. **181**(2): p. 281-292 e6.
703 15.   Sztain, T., et al., *A glycan gate controls opening of the SARS-CoV-2 spike protein.*
704   bioRxiv, 2021.
705 16.   Zhao, Z., et al., *Omicron SARS-CoV-2 mutations stabilize spike up-RBD*
706   *conformation and lead to a non-RBM-binding monoclonal antibody escape.* Nat
707   Commun, 2022. **13**(1): p. 4958.
708 17.   Whittaker, G.R., *SARS-CoV-2 spike and its adaptable furin cleavage site.* Lancet
709   Microbe, 2021. **2**(10): p. e488-e489.
710 18.   Henderson, R., et al., *Controlling the SARS-CoV-2 spike glycoprotein conformation.*
711   Nat Struct Mol Biol, 2020. **27**(10): p. 925-933.
712 19.   Wrapp, D., et al., *Cryo-EM structure of the 2019-nCoV spike in the prefusion*
713   *conformation.* Science, 2020. **367**(6483): p. 1260-1263.
714 20.   Zhang, J., et al., *Structural impact on SARS-CoV-2 spike protein by D614G*
715   *substitution.* Science, 2021. **372**(6541): p. 525-530.
716 21.   Bangaru, S., et al., *Structural analysis of full-length SARS-CoV-2 spike protein from*
717   *an advanced vaccine candidate.* Science, 2020. **370**(6520): p. 1089-1094.
718 22.   Ren, P., et al., *Function and Cryo-EM structures of broadly potent bispecific*
719   *antibodies against multiple SARS-CoV-2 Omicron sublineages.* bioRxiv, 2022.
720 23.   Liu, C., et al., *The antibody response to SARS-CoV-2 Beta underscores the antigenic*
721   *distance to other variants.* Cell Host Microbe, 2022. **30**(1): p. 53-68 e12.
722 24.   Wang, Y., et al., *Structural basis for SARS-CoV-2 Delta variant recognition of ACE2*
723   *receptor and broadly neutralizing antibodies.* Nat Commun, 2022. **13**(1): p. 871.
724 25.   Gobeil, S.M., et al., *Effect of natural mutations of SARS-CoV-2 on spike structure,*
725   *conformation, and antigenicity.* Science, 2021. **373**(6555).
726 26.   Han, P., et al., *Receptor binding and complex structures of human ACE2 to spike RBD*
727   *from omicron and delta SARS-CoV-2.* Cell, 2022. **185**(4): p. 630-640 e10.

728   27.   Saito, A., et al., *Enhanced fusogenicity and pathogenicity of SARS-CoV-2 Delta*
729   *P681R mutation.* Nature, 2022. **602**(7896): p. 300-306.
730   28.   Greaney, A.J., et al., *Complete Mapping of Mutations to the SARS-CoV-2 Spike*
731   *Receptor-Binding Domain that Escape Antibody Recognition.* Cell Host Microbe,
732   2021. **29**(1): p. 44-57 e9.
733   29.   Korber, B., et al., *Tracking Changes in SARS-CoV-2 Spike: Evidence that D614G*
734   *Increases Infectivity of the COVID-19 Virus.* Cell, 2020. **182**(4): p. 812-827 e19.
735   30.   Mansbach, R.A., et al., *The SARS-CoV-2 Spike variant D614G favors an open*
736   *conformational state.* Sci Adv, 2021. **7**(16).
737   31.   Weissman, D., et al., *D614G Spike Mutation Increases SARS CoV-2 Susceptibility to*
738   *Neutralization.* Cell Host Microbe, 2021. **29**(1): p. 23-31 e4.
739   32.   Zhang, L., et al., *SARS-CoV-2 spike-protein D614G mutation increases virion spike*
740   *density and infectivity.* Nat Commun, 2020. **11**(1): p. 6013.
741   33.   Choi, Y.K., et al., *Structure, Dynamics, Receptor Binding, and Antibody Binding of*
742   *the Fully Glycosylated Full-Length SARS-CoV-2 Spike Protein in a Viral Membrane.*
743   J Chem Theory Comput, 2021. **17**(4): p. 2479-2487.
744   34.   Li, Y., et al., *Exploring the Regulatory Function of the N-terminal Domain of SARS-*
745   *CoV-2 Spike Protein through Molecular Dynamics Simulation.* Adv Theory Simul,
746   2021. **4**(10): p. 2100152.
747   35.   Melero, R., et al., *Continuous flexibility analysis of SARS-CoV-2 spike prefusion*
748   *structures.* IUCrJ, 2020. **7**(Pt 6): p. 1059-69.
749   36.   Sinha, A. and S. Roy, *Intrinsically Disordered Regions Function as a Cervical Collar to*
750   *Remotely Regulate the Nodding Dynamics of SARS-CoV-2 Prefusion Spike Heads.* J
751   Phys Chem B, 2023. **127**(39): p. 8393-8405.
752   37.   McCallum, M., et al., *Molecular basis of immune evasion by the Delta and Kappa*
753   *SARS-CoV-2 variants.* Science, 2021. **374**(6575): p. 1621-1626.
754   38.   Shajahan, A., et al., *Deducing the N- and O-glycosylation profile of the spike protein*
755   *of novel coronavirus SARS-CoV-2.* Glycobiology, 2020. **30**(12): p. 981-988.
756   39.   Watanabe, Y., et al., *Site-specific glycan analysis of the SARS-CoV-2 spike.* Science,
757   2020. **369**(6501): p. 330-333.
758   40.   Manrique, P.D., et al., *Network analysis outlines strengths and weaknesses of*
759   *emerging SARS-CoV-2 Spike variants.* bioRxiv, 2021.
760   41.   Casalino, L., et al., *AI-Driven Multiscale Simulations Illuminate Mechanisms of*
761   *SARS-CoV-2 Spike Dynamics.* bioRxiv, 2020.
762   42.   Casalino, L., et al., *Beyond Shielding: The Roles of Glycans in the SARS-CoV-2 Spike*
763   *Protein.* ACS Cent Sci, 2020. **6**(10): p. 1722-1734.
764   43.   Mahmoudi Gomari, M., et al., *Insight into molecular characteristics of SARS-CoV-2*
765   *spike protein following D614G point mutation, a molecular dynamics study.* J Biomol
766   Struct Dyn, 2022. **40**(12): p. 5634-5642.
767   44.   Dacon, C., et al., *Broadly neutralizing antibodies target the coronavirus fusion*
768   *peptide.* Science, 2022. **377**(6607): p. 728-735.

45. Elshabrawy, H.A., et al., *Human monoclonal antibodies against highly conserved HR1 and HR2 domains of the SARS-CoV spike protein are more broadly neutralizing.* PLoS One, 2012. **7**(11): p. e50366.

46. Pang, W., et al., *A variant-proof SARS-CoV-2 vaccine targeting HR1 domain in S2 subunit of spike protein.* Cell Res, 2022.

47. Chakraborty, S., et al., *Quantification of the Resilience and Vulnerability of HIV-1 Native Glycan Shield at Atomistic Detail.* iScience, 2020. **23**(12): p. 101836.

48. Fischer, W., et al., *HIV-1 and SARS-CoV-2: Patterns in the evolution of two pandemic pathogens.* Cell Host Microbe, 2021. **29**(7): p. 1093-1110.

49. Cerutti, G., et al., *Potent SARS-CoV-2 neutralizing antibodies directed against spike N-terminal domain target a single supersite.* Cell Host Microbe, 2021. **29**(5): p. 819-833 e7.

50. Planas, D., et al., *Reduced sensitivity of SARS-CoV-2 variant Delta to antibody neutralization.* Nature, 2021. **596**(7871): p. 276-280.

51. Liu, Y., et al., *The SARS-CoV-2 Delta variant is poised to acquire complete resistance to wild-type spike vaccines.* BioRxiv, 2021.

52. Yang, T.-J., et al., *Structure-activity relationships of B. 1.617 and other SARS-CoV-2 spike variants.* BioRxiv, 2021.

53. Onodera, T., et al., *A SARS-CoV-2 antibody broadly neutralizes SARS-related coronaviruses and variants by coordinated recognition of a virus-vulnerable site.* Immunity, 2021. **54**(10): p. 2385-2398 e10.

54. Henderson, R., et al., *Glycans on the SARS-CoV-2 Spike Control the Receptor Binding Domain Conformation.* bioRxiv, 2020.

55. Zheng, L., et al., *SARS-CoV-2 spike protein receptor-binding domain N-glycans facilitate viral internalization in respiratory epithelial cells.* Biochem Biophys Res Commun, 2021. **579**: p. 69-75.

56. Seow, J., et al., *A neutralizing epitope on the SD1 domain of SARS-CoV-2 spike targeted following infection and vaccination.* Cell Rep, 2022. **40**(8): p. 111276.

57. Diaz-Salinas, M.A., et al., *Conformational dynamics and allosteric modulation of the SARS-CoV-2 spike.* Elife, 2022. **11**.

58. Liu, Y., et al., *Delta spike P681R mutation enhances SARS-CoV-2 fitness over Alpha variant.* bioRxiv, 2021.

59. Poh, C.M., et al., *Two linear epitopes on the SARS-CoV-2 spike protein that elicit neutralising antibodies in COVID-19 patients.* Nat Commun, 2020. **11**(1): p. 2806.

60. Chavda, V.P., et al., *The Delta and Omicron Variants of SARS-CoV-2: What We Know So Far.* Vaccines (Basel), 2022. **10**(11).

61. Kim, T.H., S. Bae, and J. Myoung, *Differential Impact of Spike Protein Mutations on SARS-CoV-2 Infectivity and Immune Evasion: Insights from Delta and Kappa Variants.* J Microbiol Biotechnol, 2024. **34**(12): p. 2506-2515.

62. Zhang, J., et al., *Membrane fusion and immune evasion by the spike protein of SARS-CoV-2 Delta variant.* Science, 2021. **374**(6573): p. 1353-1360.

810   63.   Humphrey, W., A. Dalke, and K. Schulten, *VMD: visual molecular dynamics.* J Mol
811   Graph, 1996. **14**(1): p. 33-8, 27-8.
812